Discovery and physical characterization of a large scattered disk object at 92 au

Article (Published Version)

The Astrophysical Journal Letters, 839:L15 (7pp), 2017 April 10 https://doi.org/10.3847/2041-8213/aa64d8

Discovery and Physical Characterization of a Large Scattered Disk Object at 92 au

D. W. Gerdes[1,2], M. Sako[3], S. Hamilton[1], K. Zhang[2], T. Khain[1], J. C. Becker[2], J. Annis[4], W. Wester[4], G. M. Bernstein[3], C. Scheibner[1,5], L. Zullo[1], F. Adams[1,2], E. Bergin[2], A. R. Walker[6], J. H. Mueller[4,7], T. M. C. Abbott[6], F. B. Abdalla[8,9], S. Allam[4], K. Bechtol[10], A. Benoit-Lévy[8,11,12], E. Bertin[11,12], D. Brooks[8], D. L. Burke[13,14], A. Carnero Rosell[15,16], M. Carrasco Kind[17,18], J. Carretero[19], C. E. Cunha[13], L. N. da Costa[15,16], S. Desai[20], H. T. Diehl[4], T. F. Eifler[21], B. Flaugher[4], J. Frieman[4,22], J. García-Bellido[23], E. Gaztanaga[24], D. A. Goldstein[25,26], D. Gruen[13,14], J. Gschwend[15,16], G. Gutierrez[4], K. Honscheid[27,28], D. J. James[6,29], S. Kent[4,22], E. Krause[13], K. Kuehn[30], N. Kuropatkin[4], O. Lahav[8], T. S. Li[4,31], M. A. G. Maia[15,16], M. March[3], J. L. Marshall[31], P. Martini[27,32], F. Menanteau[17,18], R. Miquel[19,33], R. C. Nichol[34], A. A. Plazas[21], A. K. Romer[35], A. Roodman[13,14], E. Sanchez[36], I. Sevilla-Noarbe[36], M. Smith[37], R. C. Smith[6], M. Soares-Santos[4], F. Sobreira[15,38], E. Suchyta[39], M. E. C. Swanson[18], G. Tarle[1], D. L. Tucker[4], and Y. Zhang[4]

(DES Collaboration)

[1] Department of Physics, University of Michigan, Ann Arbor, MI 48109, USA; gerdes@umich.edu
[2] Department of Astronomy, University of Michigan, Ann Arbor, MI 48109, USA
[3] Department of Physics and Astronomy, University of Pennsylvania, Philadelphia, PA 19104, USA
[4] Fermi National Accelerator Laboratory, P.O. Box 500, Batavia, IL 60510, USA
[5] Department of Physics, St. Olaf Collage, Northfield, MN 55057, USA
[6] Cerro Tololo Inter-American Observatory, National Optical Astronomy Observatory, Casilla 603, La Serena, Chile
[7] Illinois Mathematics and Science Academy, 1500 Sullivan Road, Aurora, IL 60506-1000, USA
[8] Department of Physics & Astronomy, University College London, Gower Street, London, WC1E 6BT, UK
[9] Department of Physics and Electronics, Rhodes University, P.O. Box 94, Grahamstown 6140, South Africa
[10] LSST, 933 North Cherry Avenue, Tucson, AZ 85721, USA
[11] CNRS, UMR 7095, Institut d'Astrophysique de Paris, F-75014 Paris, France
[12] Sorbonne Universités, UPMC Univ Paris 06, UMR 7095, Institut d'Astrophysique de Paris, F-75014 Paris, France
[13] Kavli Institute for Particle Astrophysics & Cosmology, P.O. Box 2450, Stanford University, Stanford, CA 94305, USA
[14] SLAC National Accelerator Laboratory, Menlo Park, CA 94025, USA
[15] Laboratório Interinstitucional de e-Astronomia—LIneA, Rua Gal. José Cristino 77, Rio de Janeiro, RJ 20921-400, Brazil
[16] Observatório Nacional, Rua Gal. José Cristino 77, Rio de Janeiro, RJ 20921-400, Brazil
[17] Department of Astronomy, University of Illinois, 1002 W. Green Street, Urbana, IL 61801, USA
[18] National Center for Supercomputing Applications, 1205 West Clark Street, Urbana, IL 61801, USA
[19] Institut de Física d'Altes Energies (IFAE), The Barcelona Institute of Science and Technology, Campus UAB, E-08193 Bellaterra (Barcelona) Spain
[20] Department of Physics, IIT Hyderabad, Kandi, Telangana 502285, India
[21] Jet Propulsion Laboratory, California Institute of Technology, 4800 Oak Grove Drive, Pasadena, CA 91109, USA
[22] Kavli Institute for Cosmological Physics, University of Chicago, Chicago, IL 60637, USA
[23] Instituto de Fisica Teorica UAM/CSIC, Universidad Autonoma de Madrid, E-28049 Madrid, Spain
[24] Institut de Ciències de l'Espai, IEEC-CSIC, Campus UAB, Carrer de Can Magrans, s/n, E-08193 Bellaterra, Barcelona, Spain
[25] Department of Astronomy, University of California, Berkeley, 501 Campbell Hall, Berkeley, CA 94720, USA
[26] Lawrence Berkeley National Laboratory, 1 Cyclotron Road, Berkeley, CA 94720, USA
[27] Center for Cosmology and Astro-Particle Physics, The Ohio State University, Columbus, OH 43210, USA
[28] Department of Physics, The Ohio State University, Columbus, OH 43210, USA
[29] Astronomy Department, University of Washington, Box 351580, Seattle, WA 98195, USA
[30] Australian Astronomical Observatory, North Ryde, NSW 2113, Australia
[31] George P. and Cynthia Woods Mitchell Institute for Fundamental Physics and Astronomy, and Department of Physics and Astronomy, Texas A&M University, College Station, TX 77843, USA
[32] Department of Astronomy, The Ohio State University, Columbus, OH 43210, USA
[33] Institució Catalana de Recerca i Estudis Avançats, E-08010 Barcelona, Spain
[34] Institute of Cosmology & Gravitation, University of Portsmouth, Portsmouth PO1 3FX, UK
[35] Department of Physics and Astronomy, Pevensey Building, University of Sussex, Brighton BN1 9QH, UK
[36] Centro de Investigaciones Energéticas, Medioambientales y Tecnológicas (CIEMAT), Madrid, Spain
[37] School of Physics and Astronomy, University of Southampton, Southampton SO17 1BJ, UK
[38] Universidade Federal do ABC, Centro de Ciências Naturais e Humanas, Av. dos Estados, 5001, Santo André, SP 09210-580, Brazil
[39] Computer Science and Mathematics Division, Oak Ridge National Laboratory, Oak Ridge, TN 37831, USA

Received 2017 February 1; revised 2017 February 27; accepted 2017 March 3; published 2017 April 12

Abstract

We report the observation and physical characterization of the possible dwarf planet 2014 UZ_{224} ("DeeDee"), a dynamically detached trans-Neptunian object discovered at 92 au. This object is currently the second-most distant known trans-Neptunian object with reported orbital elements, surpassed in distance only by the dwarf planet Eris. The object was discovered with an *r*-band magnitude of 23.0 in data collected by the Dark Energy Survey between 2014 and 2016. Its 1140 year orbit has $(a, e, i) = (109\ \mathrm{au}, 0.65, 26.^{\circ}8)$. It will reach its perihelion distance of 38 au in the year 2142. Integrations of its orbit show it to be dynamically stable on Gyr timescales, with only weak interactions with Neptune. We have performed follow-up observations with ALMA, using 3 hr of on-source integration time to measure the object's thermal emission in the Rayleigh–Jeans tail. The signal is detected at 7σ significance, from which we determine a *V*-band albedo of $13.1^{+3.3}_{-2.4}(\mathrm{stat})^{+2.0}_{-1.4}(\mathrm{sys})$ percent and a diameter of $635^{+57}_{-61}(\mathrm{stat})^{+32}_{-39}(\mathrm{sys})$ km, assuming a spherical body with uniform surface properties.

Key words: infrared: planetary systems – Kuiper belt: general – methods: observational – techniques: photometric

Supporting material: data behind figure

1. Introduction

The scattered disk and inner Oort cloud populations of trans-Neptunian objects (TNOs) extend well beyond the classical Kuiper Belt, to distances of hundreds of au. These dynamically disturbed populations must have arisen from very different mechanisms than those that produced the classical Kuiper Belt, as evidenced by marked differences in their sizes (Fraser et al. 2014), colors (Tegler & Romanishin 2000), albedos (Brucker et al. 2009), and fraction of binaries (Noll et al. 2008). The scattered disk population has been further divided by Gladman et al. (2008) into objects which are actively scattering off Neptune (as indicated by a significant variation in their semimajor axis on 10 Myr timescales), and detached objects (non-scattering, non-resonant objects with $e > 0.24$). The half-dozen longest-period members of these populations display a statistically improbable clustering in argument of perihelion and longitude of ascending node. This finding has motivated the hypothesis of a distant super-Earth (Trujillo & Sheppard 2014; Batygin & Brown 2016), sometimes called Planet 9. Deep, wide-area surveys capable of probing the distant scattered disk to high ecliptic latitudes have considerable potential to contribute to our knowledge of this region (Abbott et al. 2016). In this Letter, we report the discovery of a large scattered disk object at 92 au using data from the Dark Energy Survey (DES; Flaugher 2005), with follow-up radiometric measurements by ALMA. Of known solar system objects with reported orbital elements, only the Pluto-sized dwarf planet Eris is currently more distant.

The DES is an optical survey of 5000 square degrees of the southern sky being carried out with the Dark Energy Camera (DECam; Flaugher et al. 2015) on the 4-meter Blanco telescope at Cerro Tololo Inter-American Observatory in Chile. DECam is a prime-focus camera with a 3 square degree field of view and a focal plane consisting of 62 $2\,k \times 4\,k$ fully depleted, red-sensitive CCDs. To achieve its primary scientific goal of constraining the dark energy equation of state, the DES has been awarded 525 nights over 5 years to carry out two interleaved surveys. The DES Supernova Program (DES-SN; Bernstein et al. 2012) images 10 distinct DECam fields (a total of 30 square degrees) in the *griz* bands at approximately weekly intervals throughout the DES observing season, which runs from mid-August through mid-February. The Wide Survey covers the full survey footprint in the *grizY* bands to a limiting single-exposure depth of $m_r \sim 23.8$, with the goal of achieving 10 tilings per filter over the duration of the survey. The same combination of survey area and depth that makes DES a powerful tool for precision cosmology also makes it well suited to identify faint, distant objects in our own Solar System. With broad off-ecliptic coverage, it is especially well-suited to identifying members of the scattered disk and other high-inclination TNO populations such as detached and inner Oort cloud objects. We have previously reported on searches for TNOs in the DES-SN fields from the first two DES seasons, where discoveries have included two Neptune Trojans (Gerdes et al. 2016) and the "extreme TNO" 2013 RF_{98} (Abbott et al. 2016), whose orbital alignment with other members of its class helped motivate the Planet 9 hypothesis. This Letter presents our first result from the extension of the TNO search to the full DES Wide Survey, using data collected during the first three DES observing campaigns between 2013 August and 2016 February.

2. Optical Data and Analysis

This analysis uses data from 14,857 exposures collected in the *griz* bands during the first three DES observing campaigns (Diehl et al. 2016). These exposures cover a 2500 square degree region north of decl. $= -40$, about half the full survey area. They contain over 1.1 billion individual object detections.

We identify transient objects using a variant of the DES supernova difference-imaging pipeline, `DiffImg` (Kessler et al. 2015). Each exposure (search image) is subtracted from every other DES exposure (template image) of that region taken in the same band. We do not use template images from the same night to avoid subtracting out the most distant and slowest moving objects, which may appear stationary over a period of several hours.

The difference images created from each search-template pair are then averaged, and statistically significant sources are identified in the combined image. Subtraction artifacts are rejected using a machine-learning technique described in Goldstein et al. (2015). This typically yields ∼10 good-quality transient detections on each $9' \times 18'$ area covered by a single CCD.

After removal of stationary objects and artifacts with `DiffImg`, our search sample contains about 5 million single-epoch transients. While our selection efficiently retains true astrophysical transients—asteroids, variable stars, supernovae, etc.—the fraction of TNOs in this sample is on the order of only 0.1%.

The apparent motion of a distant solar system object over periods of several weeks is primarily due not to its own orbital motion but to parallax arising from the motion of the Earth. Our TNO search procedure begins by identifying pairs of detections within 30 nights of each other whose separation is consistent with the seasonally appropriate parallax expected for a distant object ($\lesssim 4''/\mathrm{hr}$). We then attempt to link these pairs into chains of three or more observations, testing each chain for goodness of fit to an orbit using code built on the `fit_radec` algorithm of Bernstein & Khushalani (2000, hereafter B&K) and requiring $\chi^2/N < 2$.

2014 UZ_{224} was originally detected at a heliocentric distance of 92.5 au in seven linked observations on four nights between 2014 September 27 and 2014 October 28, with an *r*-band magnitude of 23.0 and an ecliptic latitude of $-10.^{\circ}3$. The object was detected in six more DES survey images between 2014 August 19 and 2015 January 8, and was recovered in a targeted DECam observation on 2016 July 18. The motion of the object over the period of these observations is shown in Figure 1. The orbital elements are obtained using the B&K fitter. These and other data from these observations are shown in Table 1. We refer informally to this object as "DeeDee," for "distant dwarf."

Apparent and absolute magnitudes of solar system objects are often standardized to Johnson–Cousins *V*-band magnitudes. We first derived transformation equations for stellar psf magnitudes to relate DES and SDSS magnitudes, then applied the transformations of Smith et al. (2002) to convert from the SDSS

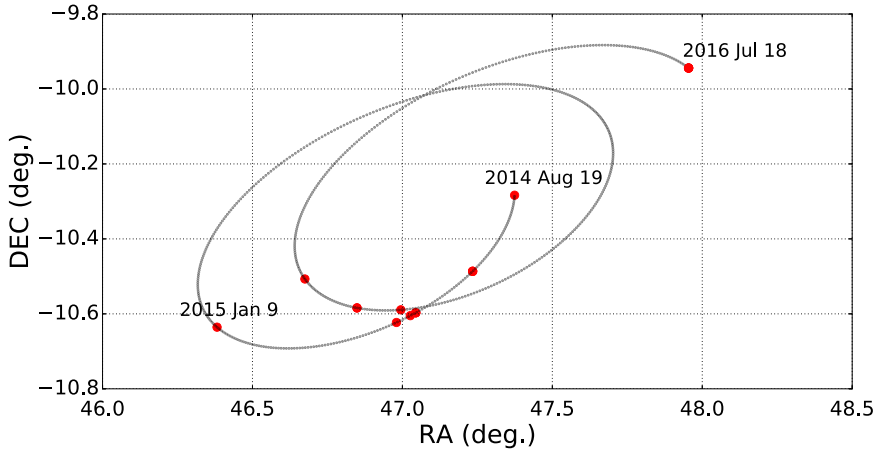

Figure 1. Path of 2014 UZ_{224} over the course of its observed 699 day arc. Dots indicate locations at which the object was observed by the DES. The data used to create this figure are available.

Table 1
Orbital Elements and Other Properties of 2014 UZ_{224}

Parameter	Value
a (au)	108.90 ± 7.36
e	0.651 ± 0.030
i (deg)	26.78509 ± 0.00012
ω (deg)	29.55 ± 1.46
Ω (deg)	131.142 ± 0.053
Perihelion (au)	37.97 ± 0.69
Perihelion date	$2142/01/02 \pm 1654$d
Aphelion (au)	179.8 ± 12.1
Period (years)	1136 ± 115
Epoch JD	2457600.5
Heliocentric distance at discovery (au)	92.5
Arc length (days)	699
Apparent mag (r)	22.98 ± 0.04
Apparent mag (V)	23.38 ± 0.05
Absolute mag H_V	3.5
$g - r$ (mag.)	0.77 ± 0.11
$r - i$ (mag.)	0.39 ± 0.07
$i - z$ (mag.)	0.22 ± 0.16
Albedo (%)	$13.1^{+3.3}_{-2.4}$(stat)$^{+2.0}_{-1.4}$(sys)
Diameter (km)	635^{+57}_{-61}(stat)$^{+32}_{-39}$(sys)

to Johnson–Cousins systems, obtaining $m_V = 23.38 \pm 0.05$. The transformation equations depend on the $g - r$ color of the object in question, which is uncertain at the level of 0.11 mag. As a cross-check, the measured spectra of five TNOs with similar colors were flux-corrected and found to have a reasonable match to the observed DES magnitudes. From the flux-calibrated spectra of each of these TNOs, we applied a synthetic determination of the V-band magnitude. The central value and spread of these values are consistent with our measurement.

3. Orbital Dynamics

We next investigated the dynamical behavior of 2014 UZ_{224} on Gyr timescales. We generated 100,000 clones of 2014 UZ_{224} with respect to the best-fit orbit and its covariance matrix as described in Gladman et al. (2008). Taking the clone with the smallest rms residual to be the new best fit, we repeated the clone-generating procedure and identified the clones that yield residuals consistent with observations. Out of these objects, we chose the clones with minimum and maximum semimajor axes, as well as five additional clones interspersed between those two, and numerically integrated the solar system using all eight clones as test particles. We ran the integration for 1 Gyr using the hybrid symplectic and Bulirsch-Stoer integrator built into `Mercury6` (Chambers 1999) and conserved energy to 1 part in 10^9. We did not include the terrestrial planets in our integrations, and we replaced Jupiter, Saturn, and Uranus with a solar J_2 (as done in Batygin & Brown 2016). We included Neptune as an active body because 2014 UZ_{224}'s perihelion distance of 38 au brings it into proximity with Neptune.

As shown in Figure 2, over 1 Gyr timescales each clone remains confined to a region closely surrounding its measured orbit, with $\delta a/a$ being less than 1% for all clones. This result indicates that despite the potentially destabilizing interactions with Neptune, this object remains dynamically stable and satisfies the formal criteria of Gladman et al. (2008) as a detached TNO. Although the uncertainty on the object's semimajor axis overlaps with the 7:1 mean-motion resonance with Neptune, none of the clones we examined undergoes libration. We also performed several 4.5 Gyr integrations of the best-fit orbit. The object demonstrated stability over the full solar system lifetime as well.

4. Measurement of Thermal Emission, Size, and Albedo

We observed 2014 UZ_{224} with director's discretionary time on the Atacama Large Millimeter/submillimeter Array (ALMA) on 2016 August 19 and 20. The observations were carried out with 41 antennae and baselines between 15 and 1462 m. The source was tracked using a user-provided ephemeris. The correlator was configured to observe four continuum spectral windows centered on 224, 226, 240, and 242 GHz, respectively, resulting in a total bandwidth of 7.5 GHz. The nearby quasars J0522–3627 and J0238+1636 were used as bandpass calibrators for the first night and the second observations, respectively. The amplitude and phase of observations were calibrated by J0257–1212, and J0423-0120 was used for absolute flux calibration. The total on-source integration time was 176 minutes.

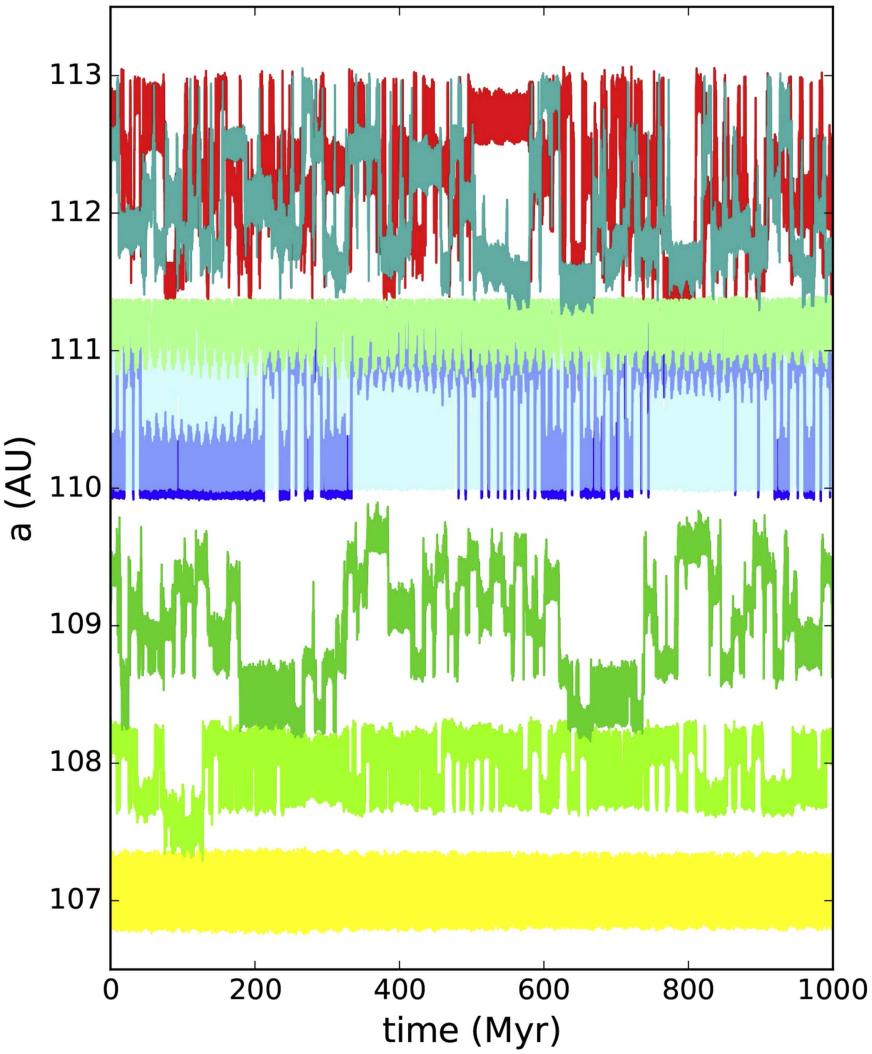

Figure 2. Time evolution of semimajor axis over 1 Gyr for each of the eight clones of 2014 UZ_{224} considered in this work, from the minimum (bottom line) to maximum (top) initial semimajor axis. For all clones, $\delta a/a$ is less than 1% in amplitude, demonstrating the long-term dynamical stability of this object in the presence of Neptune.

The raw data were calibrated by NRAO staff manually using the CASA package version 4.6. The calibrated visibilities of five data sets were then stacked to align the position using the `fixplanet` command. We generated a synthesized continuum image with the CLEAN algorithm and a natural weighting in CASA. The resulting synthesized beam is $0\farcs30 \times 0\farcs25$, with a position angle of $-84°$. A bright point-like source is detected at the center of the image, with a peak flux of 47 μJy/beam and a signal-to-noise ratio of $\sim$7. We used the `imfit` task in CASA to fit the central source with a 2D Gaussian and found the source had a major-axis FWHM of $0.33 \pm 0\farcs05$ and a minor-axis FWHM of $0.25 \pm 0\farcs03$, with a position angle of 39°. The apparent source size is thus consistent with the result of a point source convolved with the synthesized beam. The total flux measured from a 2D Gaussian fit is 53 ± 10 μJy. The final calibrated image is shown in Figure 3.

The source appears to be slightly elongated in the north–south direction compared to the synthesized beam. To test whether this apparent elongation was a result of a binary system, we fit the source with two models: a single-point-source model and a binary model. The residuals after subtracting either model are very similar, and both were within 1σ of the distribution of noise measured in the background regions of the synthesized image. We conclude that the observations are consistent with a single point source.

The combination of optical and thermal measurements allows for constraints on the object's physical properties, under the assumption of a thermal model with temperature distribution $T(\theta, \phi)$, where θ and ϕ are the planetographic coordinates on the object. The physical properties of primary interest are the object's size and albedo, which can be uniquely determined by simultaneously solving the following equations:

$$F_V = F_{\odot,V}\frac{p_V}{4}\left(\frac{D}{\Delta}\right)^2\left(\frac{r}{1\ \mathrm{au}}\right)^{-2}, \quad (1)$$

$$F_\lambda = \int \epsilon_\lambda B_\lambda(T(\theta, \phi))d\Omega, \quad (2)$$

where F_V, $F_{\odot,V}$, and F_λ are the visible, solar visible, and thermal flux densities; D is the diameter; p_V is the geometric visible albedo; r and Δ are the heliocentric and geocentric distances, respectively; ϵ_λ is the spectral emissivity; B_λ is the Planck

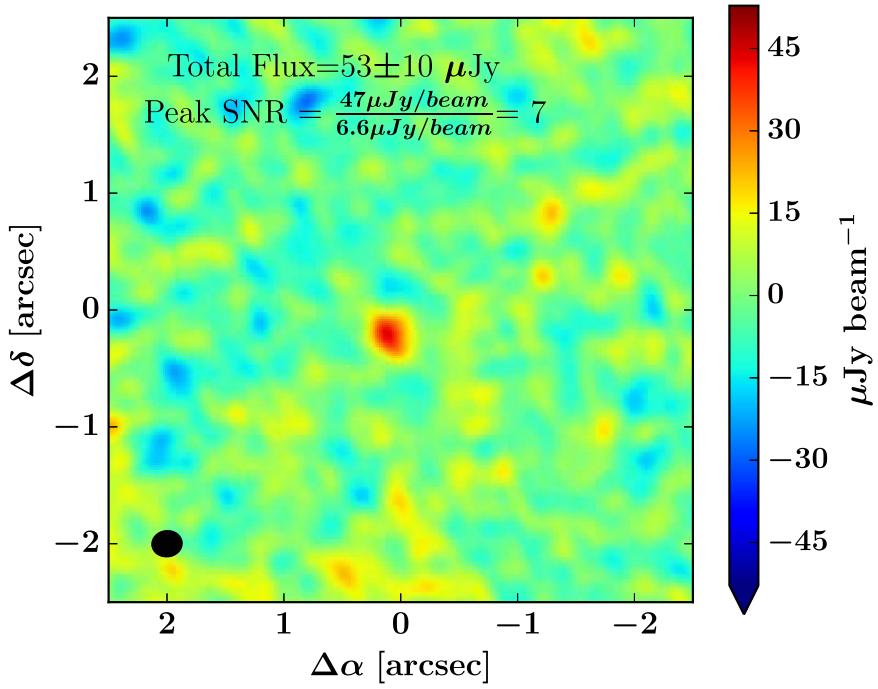

Figure 3. Calibrated, stacked image of 2014 UZ_{224} from 3 hr of on-source integration with ALMA. The black ellipse represents the size of the synthesized beam.

function; and $d\Omega$ is the solid angle subtended by the elements $d\theta$ and dϕ as seen from Earth. The form of $T = T(\theta, \phi)$ depends on the surface geography, spin rate, bolometric emissivity (ϵ), thermal inertia, and shape of the object; none of which is generally known. Therefore, it is common practice to assume a simplified thermal model.

The Standard Thermal Model (STM; Lebofsky & Spencer 1989 and references therein) describes a spherical, non-rotating body observed at zero phase angle and represents the hottest possible temperature distribution. In this model, the temperature depends only on the angular distance θ from the subsolar point where $T(\theta) = T_{SS}\cos^{1/4}\theta$ with $T_{SS} = [(1-A)S_{\odot}/(\epsilon\eta\sigma r^2)]^{1/4}$ and $T = 0$ on the nightside. Here, $A = qp_V$ is the Bond albedo and q is the phase integral. $S_{\odot}$ is the solar constant and η is the "beaming factor." η was originally introduced to account for surface roughness and variations in thermal inertia but also serves to interpolate between the STM and its "cold" counterpart, the Fast Rotator Model (FRM), by scaling the subsolar temperature. In particular, $\eta < 1$ results in a higher temperature than predicted by the model while $\eta > 1$ results in a lower predicted temperature.

Obtaining several measurements spanning both sides of the peak of the blackbody emission spectrum would allow us to leave η as a free parameter to fit in our model, significantly constraining the temperature distribution on the surface. However, this is not possible with a single-wavelength measurement, and we must allow η to explore its full range of 0.6 to 2.6 (Mommert et al. 2012). For the remainder of this work we use the STM as our base thermal model, but we allow η to take any value within its allowed range. Equation (2) then becomes

$$F_{\lambda} = \frac{\epsilon_{\lambda} D^2}{2\Delta^2}\int_0^{\pi/2} B_{\lambda}(T(\theta))\sin\theta\cos\theta d\theta. \quad (3)$$

Adopting the STM requires some assumptions regarding the nature of the object's thermal emissions. First, we assume a bolometric emissivity $\epsilon = 0.9 \pm 0.1$, a typical assumption for TNO thermal models. While the thermal emissivity can be treated as constant at wavelengths $\lesssim$350 μm, Fornasier et al. (2013) showed that the thermal emissivity is suppressed at longer wavelengths, such as the 1.3 mm wavelength corresponding to ALMA's 233 GHz band used in our measurement. We adopt a value of $\epsilon_{\lambda} = 0.68$ at 1.3 mm, the average value measured by Brown & Butler (2017) with ALMA at 233 GHz for four TNOs with sizes comparable to 2014 UZ_{224}. We keep $\epsilon = 0.9 \pm 0.1$ as our bolometric emissivity in the surface temperature distribution. Second, we assume that the phase integral $q = 0.8$ as derived in Stansberry et al. (2008) for large, bright TNOs. Varying q from 0.4 to 0.8 results in <1% variation in albedo for low-albedo TNOs. The phase angle for an object at ~92 au never exceeds 1°; thus, we may neglect any effects arising from a changing phase angle and set the phase angle equal to zero.

Estimation of the uncertainties in the calculated diameter and albedo were performed following the procedure outlined in Mommert et al. (2012). We employed a Monte Carlo simulation using 1000 clones, where each clone was generated by varying the observed flux densities at both the thermal and optical wavelengths, the heliocentric and geocentric distances associated with the optical measurements, the bolometric emissivity ϵ, and the beaming factor η. Our uncertainties are dominated by the statistical uncertainty in our flux measurements. Each parameter, with the exception of η, was varied randomly according to a normal distribution defined by its nominal value and 1σ uncertainty. η was varied according to a uniform distribution from 0.6 to 2.6. The uncertainties in the diameter and albedo were then defined by the lower and upper values that included 68.2% of the clones, centered on the peaks of the resulting distributions of the two parameters.

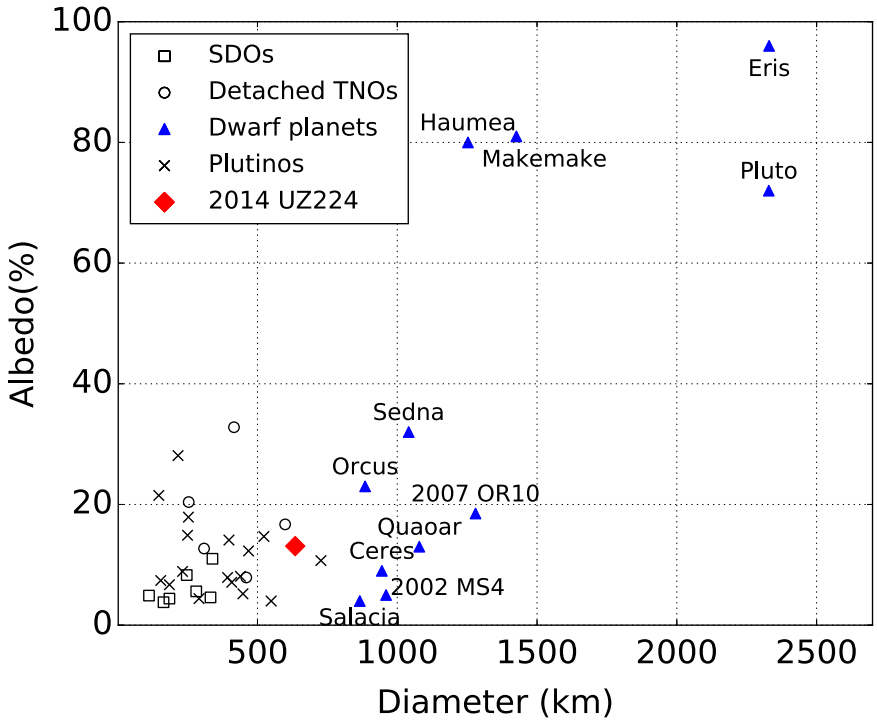

Figure 4. Size–albedo relations for selected TNO populations including detached and scattered disk objects (Li et al. 2006; Santos-Sanz et al. 2012), Plutinos (Mommert et al. 2012), and dwarf planets (Sicardy et al. 2011; Pál et al. 2012; Fornasier et al. 2013; Buratti et al. 2017; Brown & Butler 2017). The object 2014 UZ_{224} is shown as a filled diamond.

Under these assumptions, we measure the geometric albedo and diameter of 2014 UZ_{224} to be

$$p_V = 13.1^{+3.3}_{-2.4}\,(\mathrm{stat})^{+2.0}_{-1.4}\,(\mathrm{sys})\,\%$$
$$D = 635^{+57}_{-61}\,(\mathrm{stat})^{+32}_{-39}\,(\mathrm{sys})\ \mathrm{km}.$$

Here, the quoted statistical uncertainty is due to the uncertainties in both the visual and thermal flux measurements, as well as uncertainties in the helio- and geocentric distance measurements. The quoted systematic uncertainty is due to variation of the model parameters η and ϵ.

As shown in Figure 4, the measured albedo is higher than that of rocky bodies such as asteroids, and of typical classical KBOs, yet notably smaller than ice-rich dwarf planets Eris (96%; Sicardy et al. 2011), Haumea (80%; Fornasier et al. 2013), Pluto (72%; Buratti et al. 2017), and Sedna (32%; Pál et al. 2012), suggesting that 2014 UZ_{224} has a mixed ice-rock composition. An object of this composition and size is likely to have enough self-gravity to reach an approximately spherical shape in hydrostatic equilibrium (Tancredi & Favre 2008), making 2014 UZ_{224} a candidate dwarf planet.

5. Conclusions

We have reported the discovery of 2014 UZ_{224} ("DeeDee") a trans-Neptunian object discovered at 92 au from the Sun. This object has an estimated size $D = 635 \pm 70$ km and albedo $p_V = 13 \pm 4\%$, and is most likely a dwarf planet with a mixed ice-rock composition. This discovery adds to the growing inventory of dwarf planets in the outer solar system and indicates that the TNO population displays a nearly continuous distribution of size and albedo.

Neither the orbital nor the physical properties of 2014 UZ_{224} are surprising, as they are in the range of other well-characterized detached TNOs discovered closer to the Sun. The population of detected TNOs is of course strongly biased toward those that are large, near perihelion, and/or have high albedo. Current surveys such as the DES now have the depth and area coverage to discover the counterparts of known objects that are well beyond perihelion. It is also noteworthy that the ALMA facility is easily capable of radiometric detection of a 600 km body at >90 au distance. Hence, it will be possible to establish sizes and albedos for nearly every body detectable in the visible by DES and similar surveys. As these surveys progress, we will be able, for example, to determine whether the very high albedo of Eris is characteristic of large bodies at this distance, or whether flux selection has led to the first discovery being atypical.

D.W.G. and F.C.A. are partially supported by NSF grant AST-1515015. G.M.B. and M.S. are partially supported by NSF grant AST-1515804. S.J.H. and J.C.B. are supported by NSF-GRFP grant DGE-1256260. This work used the Extreme Science and Engineering Discovery Environment (NSF grant number ACI-1053575).

Funding for the DES Projects has been provided by the DOE and NSF(USA), MEC/MICINN/ MINECO (Spain), STFC (UK), HEFCE (UK), NCSA (UIUC), KICP (U. Chicago), CCAPP (Ohio State), MIFPA (Texas A&M), CNPQ, FAPERJ, FINEP (Brazil), DFG (Germany) and the Collaborating Institutions in the Dark Energy Survey.

The Collaborating Institutions are Argonne Lab, UC Santa Cruz, University of Cambridge, CIEMAT-Madrid, University of Chicago, University College London, DES-Brazil Consortium, University of Edinburgh, ETH Zürich, Fermilab, University of Illinois, *ICE* (IEEC-CSIC), IFAE Barcelona, Lawrence Berkeley Lab, LMU München and the associated Excellence Cluster Universe, University of Michigan, NOAO,

University of Nottingham, Ohio State University, University of Pennsylvania, University of Portsmouth, SLAC National Lab, Stanford University, University of Sussex, Texas A&M University, and the OzDES Membership Consortium.

The DES Data Management System is supported by the NSF under grant number AST-1138766. The DES participants from Spanish institutions are partially supported by MINECO under grants AYA2012-39559, ESP2013-48274, FPA2013-47986, and Centro de Excelencia Severo Ochoa SEV-2012-0234. Research leading to these results has received funding from the ERC under the EU's 7th Framework Programme including grants ERC 240672, 291329 and 306478.

This paper makes use of the following ALMA data: ADS/JAO.ALMA#2015.A.00023.S. ALMA is a partnership of ESO (representing its member states), NSF (USA) and NINS (Japan), together with NRC (Canada), NSC and ASIAA (Taiwan), and KASI (Republic of Korea), in cooperation with the Republic of Chile. The Joint ALMA Observatory is operated by ESO, AUI/NRAO and NAOJ. The National Radio Astronomy Observatory is a facility of the National Science Foundation operated under cooperative agreement by Associated Universities, Inc.

Software: Astropy (The Astropy Collaboration et al. 2013), Matplotlib (Hunter 2007), Numpy (Van Der Walt et al. 2011), Pandas (McKinney 2010).

References

Abbott, T., Abdalla, F. B., Aleksić, J., et al. 2016, MNRAS, 460, 1270
Batygin, K., & Brown, M. E. 2016, AJ, 151, 22
Bernstein, G., & Khushalani, B. 2000, AJ, 120, 3323
Bernstein, J. P., Kessler, R., Kuhlmann, S., et al. 2012, ApJ, 753, 152
Brown, M. E., & Butler, B. J. 2017, arXiv:0707.3168
Brucker, M. J., Grundy, W. M., Stansberry, J. A., et al. 2009, Icar, 201, 284
Buratti, B. J., Hofgartner, J. D., Hicks, M. D., et al. 2017, Icar, 287, 207
Chambers, J. E. 1999, MNRAS, 304, 793
Diehl, H. T., Neilsen, E., Gruendl, R., et al. 2016, Proc. SPIE, 9910, 99101D
Flaugher, B. 2005, IJMPA, 20, 3121
Flaugher, B., Diehl, H. T., Honscheid, K., et al. 2015, AJ, 150, 150
Fornasier, S., Lellouch, E., Müller, T., et al. 2013, A&A, 555, A15
Fraser, W. C., Brown, M. E., Morbidelli, A., Parker, A., & Batygin, K. 2014, ApJ, 782, 100
Gerdes, D. W., Jennings, R. J., Bernstein, G. M., et al. 2016, AJ, 151, 39
Gladman, B., Marsden, B. G., & Vanlaerhoven, C. 2008, in The Solar System Beyond Neptune, ed. M. A. Barucci et al. (Tucson, AZ: Univ. Arizona Press), 43
Goldstein, D. A., D'Andrea, C. B., Fischer, J. A., et al. 2015, AJ, 150, 82
Hunter, J. D. 2007, CSE, 9, 90
Kessler, R., Marriner, J., Childress, M., et al. 2015, AJ, 150, 172
Lebofsky, L. A., & Spencer, J. R. 1989, in Asteroids II, ed. R. P. Binzel, T. Gehrels, & M. S. Matthews (Tucson, AZ: Univ. Arizona Press), 128
Li, J.-Y., McFadden, L. A., Parker, J. W., et al. 2006, Icar, 182, 143
McKinney, W. 2010, in Proc. 9th Python in Science Conf., ed. S. van der Walt & J. Millman, 51, http://conference.scipy.org/proceedings/scipy2010/mckinney.html
Mommert, M., Harris, A. W., Kiss, C., et al. 2012, A&A, 541, A93
Noll, K. S., Grundy, W. M., Stephens, D. C., Levison, H. F., & Kern, S. D. 2008, Icar, 194, 758
Pál, A., Kiss, C., Müller, T. G., et al. 2012, A&A, 541, L6
Santos-Sanz, P., Lellouch, E., Fornasier, S., et al. 2012, A&A, 541, A92
Sicardy, B., Ortiz, J. L., Assafin, M., et al. 2011, Natur, 478, 493
Smith, J. A., Tucker, D. L., Kent, S., et al. 2002, AJ, 123, 2121
Stansberry, J., Grundy, W., Brown, M., et al. 2008, in The Solar System Beyond Neptune, ed. M. A. Barucci et al. (Tucson, AZ: Univ. Arizona Press), 161
Tancredi, G., & Favre, S. 2008, Icar, 195, 851
Tegler, S. C., & Romanishin, W. 2000, Natur, 407, 979
The Astropy Collaboration, Robitaille, T. P., Tollerud, E. J., et al. 2013, A&A, 558, A33
Trujillo, C. A., & Sheppard, S. S. 2014, Natur, 507, 471
Van Der Walt, S., Colbert, S. C., & Varoquaux, G. 2011, arXiv:1102.1523